Efficacy of seaweed-based carbon dioxide removal reduced by iron limitation and nutrient competition with phytoplankton

Manon Berger[1*], Lester Kwiatkowski[2†], Laurent Bopp[1†], David T. Ho[3,4†]

[1*]Department of Geosciences, LMD/ENS/IPSL, 24 rue Lhomond, Paris, 75005, France.

[2]LOCEAN/IPSL, 4 Pl. Jussieu, Paris, 75005, France.

[3]Department of Oceanography, University of Hawaii at Mānoa, 1000 Pope Road, Honolulu, HI 96822, USA.

[4][C]Worthy, Boulder, CO 80302, USA.

*Corresponding author(s). E-mail(s): manon.berger@lmd.ipsl.fr;
Contributing authors: lester.morgan-kwiatkowski@locean.ipsl.fr; bopp@lmd.ipsl.fr; ho@hawaii.edu;
[†]These authors contributed equally to this work.

Abstract

Carbon dioxide removal (CDR) is a crucial component of climate change mitigation strategies, and ocean afforestation via seaweed cultivation has been touted as a promising marine CDR (mCDR) approach due to high productivity and favorable carbon-to-nutrient ratios. However, global mCDR models generally overlook iron limitation, a potential bottleneck for sustainable seaweed cultivation. While competition with phytoplankton for nutrients could even reduce ocean carbon uptake. Here we assess the potential for this unintended consequence using an ocean biogeochemical model. We find that iron limitation reduces afforestation potential three-fold after already accounting for N and P limitation. Variations in nutrient dynamics contribute to substantial uncertainty in projections of CDR efficiency, with global CDR efficiency ranging from -43% to +78%. This study underscores the need for iron dynamics to be included in projections of ocean afforestation. Failing to account for such nutrient dynamics risks overestimating the efficacy of seaweed-based CDR as a mitigation strategy.

150 words/150

Keywords: Carbon Dioxide Removal, Ocean Afforestation, Seaweed Cultivation, seaweed, Nutrient Competition, Efficiency, Iron Limitation

1 Introduction

In response to the urgent challenge posed by climate change, strategies aimed at limiting global warming to 1.5 or 2°C by 2100 require substantial deployment of carbon dioxide removal (CDR), with projected targets ranging from 24 to 860 $GtCO_2$ throughout the 21st century [1]. One proposed CDR technique is seaweed cultivation, which is based on upscaling well-established coastal seaweed aquaculture to the near-shore open ocean, followed by the export of the harvested biomass to the deep ocean. The potentially high carbon fixation capacity of seaweed makes it an attractive option for CDR [2, 3]. However, the CDR potential and possible side effects of seaweed cultivation are poorly characterized [4, 5].

Notably, recent research has identified iron limitation as a possible bottleneck for sustainable seaweed cultivation [6]. However, iron dynamics have yet to be incorporated into seaweed-based CDR projections, which have focused on nitrate and phosphate macronutrient constraints. As a vital micronutrient, iron is required for essential metabolic functions of seaweed, including photosynthesis, growth, and nitrogen assimilation [7]. Iron also limits phytoplankton production in many ocean regions [8].

Nutrient (nitrate (N), phosphate (P), and iron (Fe)) stoichiometry (i.e. demands) and uptake affinities influence seaweed-phytoplankton competition dynamics, determining the CDR benefit of seaweed [9]. If seaweed are less nutrient efficient than phytoplankton, they could theoretically result in negative CDR. If the assessed scope of nutrient demands and affinities were limited, it could bias assessments of seaweed cultivation potential. Yet, studies that examined the CDR potential of seaweed cultivation have generally tested a limited scope of stoichiometry (e.g., C:N ratios of 16.3 and 20 (and +/- 10%), and C:P ratios of 49 and 111, as reported by Berger et al. [10] and Wu et al. [11], respectively) and one nutrient affinity, and those that have tested variable nutrient affinity have focused on seaweed production potential and overlooked geochemical and biological feedback mechanisms that influence CDR [12]. As such, there are currently poor constraints on the CDR potential of seaweed cultivation, its environmental co-benefits and consequences, and the potential optimum regions for deployment [9, 13].

This modeling study is the first to examine the effects of iron limitation [6, 9], nutrient demands, and affinities on ocean afforestation potential and CDR efficiency. Together, these two factors define the overall CDR potential of seaweed cultivation, i.e. product of the ocean afforestation potential (the amount of seaweed that can be grown) and the CDR efficiency (the amount of atmospheric carbon removed per ton of seaweed biomass) [13]. We conduct an ensemble of simulations exploring the influence of nutrient limitation, affinity, and demand on seaweed CDR in Exclusive Economic

Zones (EEZs) of the global ocean. Specifically, we assess how nutrient limitations, affinities, and demands affect phytoplankton and the overall ocean afforestation capacity and CDR efficiency.

We used a modified version of the global ocean biogeochemical model NEMO-PISCES to simulate seaweed cultivation, accounting for dissolved inorganic carbon (DIC) and nutrient uptake based on light, temperature, and nutrient availability. We simulated 25 years of cultivation in EEZs followed by 50 years of cessation under a high-mitigation scenario (Representative Concentration Pathway 2.6; RCP2.6) for the period 2025-2100. The choice of RCP2.6 reflects the consensus that CDR approaches should target eliminating residual emissions alongside substantial reductions in CO_2 emissions [1]. With the exception of afforestation potential simulations, seaweed production is scaled by enhancing afforestation in nutrient-rich regions to achieve a global production target of 0.5 PgC yr^{-1}. This ensures CDR efficiency and environmental impact comparisons are performed at a consistent afforestation level. To assess the impact of nutrient demands and affinities on CDR potential, we compiled published data on stoichiometric ratios extending the work of Sheppard et al [9] with C:Fe ratios (Fig. 1). We performed an ensemble of simulations that encapsulated the observed range in seaweed stoichiometry and nutrient uptake kinetics.

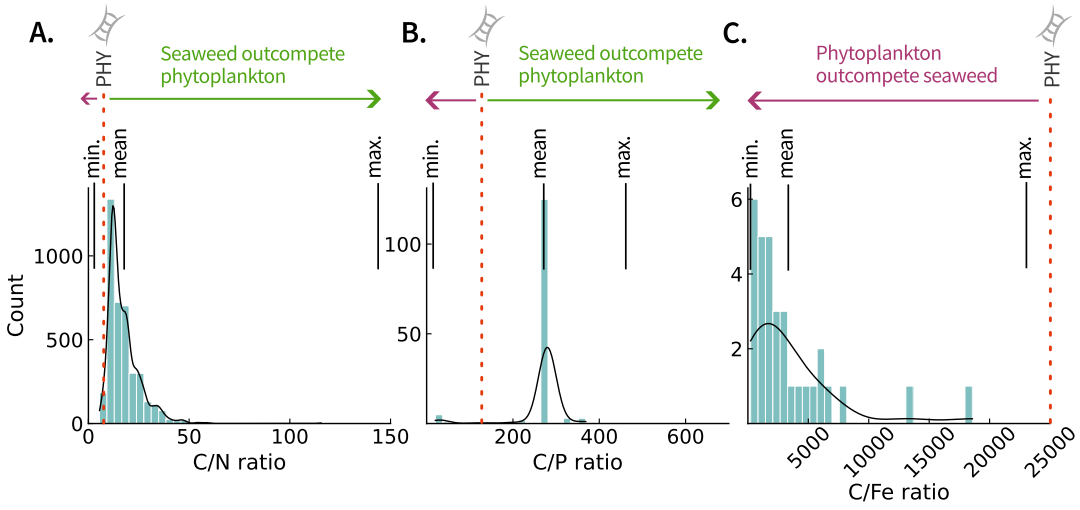

Fig. 1 Seaweed nutrient demand compared to phytoplankton. The carbon to (**A**) nitrogen, (**B**) phosphorus, and (**C**) iron ratios. High carbon-to-nutrient ratios correspond to a low nutrient demand for carbon fixation. Seaweed mean, maximal (max.), and minimal (min.) carbon-to-nutrient ratios are shown. Bounds are 25% greater (lower) than the maximum (minimum) biological parameter values found in the literature. Dotted red lines represent phytoplankton carbon-to-nutrient ratios used in the PISCES model, specifically the Redfield ratios for nitrogen and phosphorus (C:N and C:P) and the minimum carbon-to-iron quota (C:Fe) (the carbon-to-iron quota in PISCES varies from 25,000 to 1,000,000).

2 Results

2.1 Ocean afforestation potential is limited by iron

Nitrogen and phosphorus limitations constrain ocean afforestation potential, confining high production areas primarily to high latitudes, and upwelling regions. N and P limitations on seaweed growth (simulation CNP) reduce ocean afforestation potential compared to the idealized afforestation potential without nutrient constraints (simulation C), with only 15% of the idealized afforestation potential achieved after 25 years of cultivation (Fig. 2 a and b). Mid-latitude regions are most affected, with production reduced by 80–100%. Approximately 36% of the cultivation area experiences near-total production loss, with reductions exceeding 95% relative to the idealized potential. In contrast, high-latitude and upwelling regions maintained near-complete production.

The inclusion of iron limitation further diminishes afforestation potential, with only 5% of the idealized capacity realized (Fig. 2 a and c). Concurrent N, P, and Fe limitation (simulation CNPFe), therefore reduces afforestation potential by a factor of three compared to the simulation where only macronutrient limitations are considered (simulation CNP). This limitation further suppresses production in high latitudes and upwelling regions, confining viable cultivation primarily to coastal zones. Pacific islands exhibit a production decline of 90% to the complete absence of production, while the Southern Ocean shows reductions of 90–99%, except in coastal areas. Overall, 63% of the cultivation area faces near-total production loss, with reductions exceeding 95% relative to the scenario without nutrient limitation. Only a limited number of coastal regions maintain viable production.

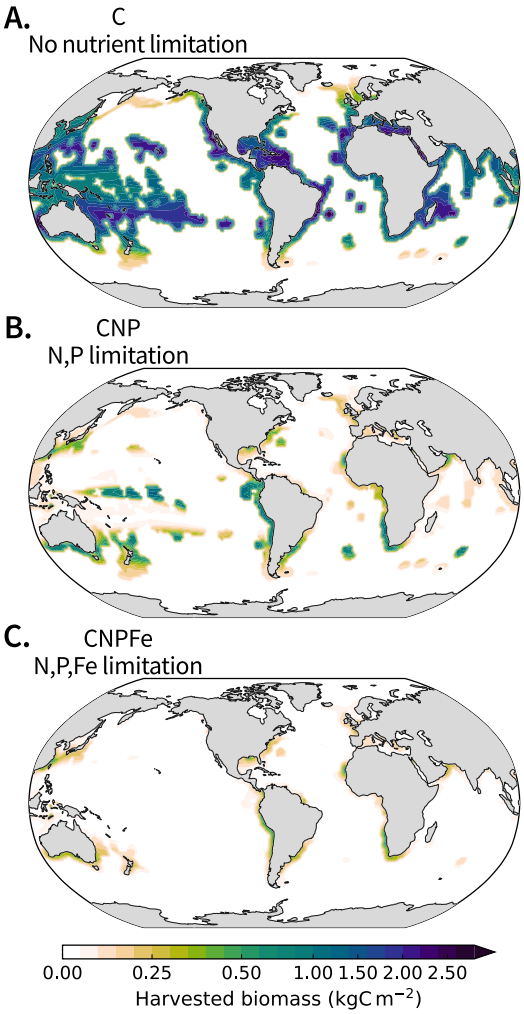

Fig. 2 Impact of nutrient limitation on afforestation potential. Maps of cumulative seaweed production (kgC m^{-2}) after 25 years of cultivation under three nutrient limitation scenarios: (**A**) no nutrient limitation (simulation C; limited only by temperature and light), (**B**) nitrate and phosphate limitation (simulation CNP), and (**C**) nitrate, phosphate, and iron limitation (simulation CNPFe).

2.2 Seaweed CDR is counterproductive in 20% of the ocean when iron is accounted for

Seaweed-based CDR generally enhances ocean carbon uptake, but its effectiveness is strongly influenced by nutrient limitations, which can sometimes cause a reduction in the ocean carbon sink. In the absence of nutrient constraints, seaweed cultivation causes an additional carbon flux of up to 1.76 $GtCO_2$ yr^{-1} (0.48 GtC yr^{-1}) for global seaweed production of 0.5 GtC yr^{-1}, equivalent to 1.83 $GtCO_2$ yr^{-1} (Fig. 3, simulation C). This represents a CDR efficiency of 82% after 25 years of cultivation and 99% after 50 years post-cessation. Macronutrient limitations reduce the maximum CDR flux to 1.66 $GtCO_2$ yr^{-1} (0.37 GtC yr^{-1}), despite maintaining the same global seaweed production of 0.5 GtC yr^{-1} (Fig. 3, simulation CNP). This reduction is driven by the

negative biological feedback associated with a decline in phytoplankton primary production due to nutrient diversion (Fig. 4). Consequently, the CDR efficiency decreases to 64% after 25 years of cultivation and only 81% after 50 years post-cessation. The inclusion of iron limitation further lowers the CDR flux to 0.73 $GtCO_2$ yr^{-1} (0.2 GtC yr^{-1}), with seaweed production remaining at 0.5 GtC yr^{-1} (Fig. 3, simulation CNPFe) due to enhanced biological feedback. Under these constraints, CDR efficiency drops to 24% after 25 years and recovers only to 60% after 50 years post-cessation.

Regionally, in the absence of nutrient limitations, the CDR flux is relatively uniform (Fig. 3 D), aligning with areas of maximum afforestation potential (Fig. 2 A). When macronutrient limitations are considered, the highest CDR fluxes occur in regions of maximum afforestation potential and nutrient-rich areas, particularly in the Southern Ocean and upwelling zones, with fluxes reaching up to 52 gCO_2 m^{-2} yr^{-1} The inclusion of iron limitation, however, causes a substantial shift, with approximately 20% of the ocean exhibiting negative CDR fluxes, including many regions that had previously exhibited high CDR fluxes under N and P limitation. In these areas, instead of enhancing carbon uptake, seaweed cultivation results in a net reduction in ocean carbon uptake. For example, the Pacific eastern boundary upwelling zone shows a negative CDR flux of up to -50 gCO_2 m^{-2} yr^{-1}. Under combined N, P, and Fe limitations, the highest CDR fluxes are found in the Northwest Pacific and Northeast Atlantic, where local fluxes reach up to 29 gCO_2 m^{-2} yr^{-1}.

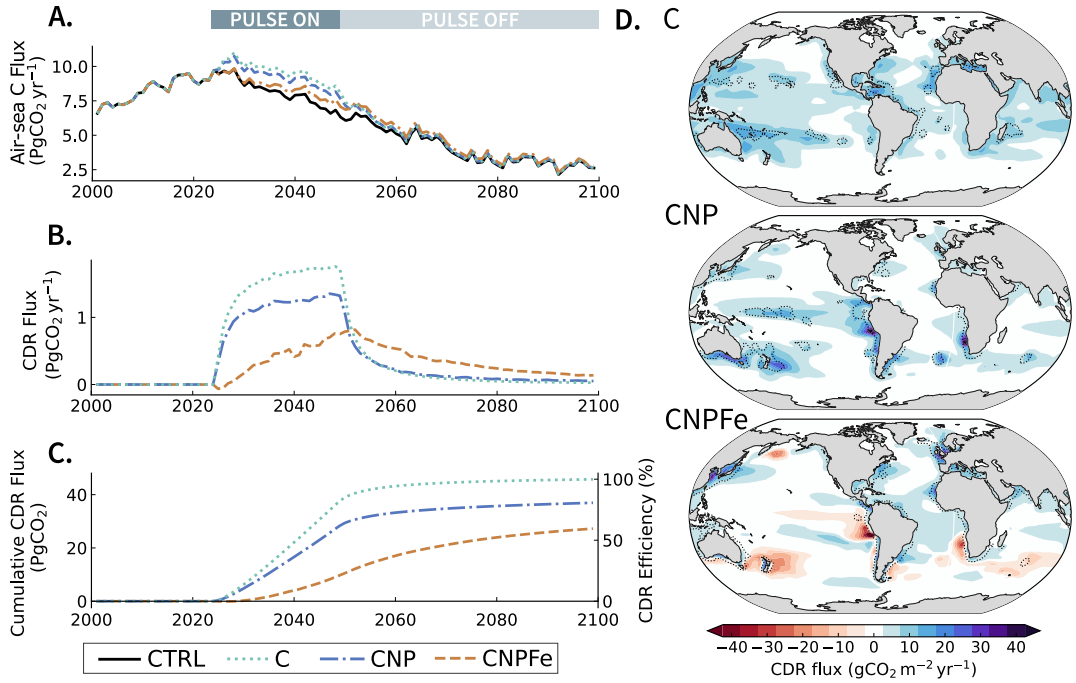

Fig. 3 Impact of nutrient limitation on CDR flux and efficiency. Time series of (**A**) total air-sea carbon flux in the control simulation (RCP2.6 scenario) and in seaweed cultivation simulations under three nutrient limitation scenarios: no nutrient limitation (C; limited only by temperature and light), nitrate and phosphate (CNP), and nitrate, phosphate, and iron (CNPFe). (**B**) CDR flux in these scenarios; (**C**) cumulative CDR flux and CDR efficiency. (**D**) Maps of the CDR flux (gCO_2 m^{-2} yr^{-1}) for C, CNP, and CNPFe, averaged over 25 years of cultivation. Dashed lines represent the threshold of 0.15 kgC m^{-2} yr^{-1} for seaweed production.

2.3 Iron amplifies the biological feedback limiting seaweed CDR efficiency

Under macronutrient limitation, a decrease in carbon export flux of up to 0.31 PgC yr^{-1} (4% decline) is observed after 25 years of cultivation compared to the control (Fig. 4, CNP). The cumulative flux reaches -6.1 PgC after 25 years of cultivation and -9.2 PgC 50 years after cessation. This reflects a reduction in carbon sequestration by the biological carbon pump (BCP), resulting in diminished CDR efficiency due to seaweed nutrient consumption (Fig. 3 C).

The introduction of iron limitation further exacerbates this reduction of the carbon export flux to 0.45 PgC yr^{-1} (5.8% decline) reached during the second year of cultivation (Fig. 4, CNPFe). After cultivation ends, the carbon export flux recovers quickly, rising by 0.28 PgC yr^{-1} within two years. Despite the rebound, cumulative carbon export flux under N, P, and Fe limitations decreases by 14.4 PgC after 25 years of cultivation and recovers to only 10.6 PgC 50 years after cessation, with most recovery occurring within the first 15 years.

Regionally, reductions in carbon export flux under N and P limitations are most pronounced in the western equatorial Pacific, where fluxes decrease by 12.0 gC m^{-2} yr^{-1} (Fig.4 D), aligning with

the decline in NPP_{PHY} (Fig.5 C and D). The inclusion of iron limitation leads to further reductions, with carbon export fluxes dropping by up to 60 gC m^{-2} yr^{-1}, particularly in the Southern Ocean and along eastern boundary currents. In contrast, certain subtropical regions show an increase in carbon export flux of up to 10 gC m^{-2} yr^{-1}.

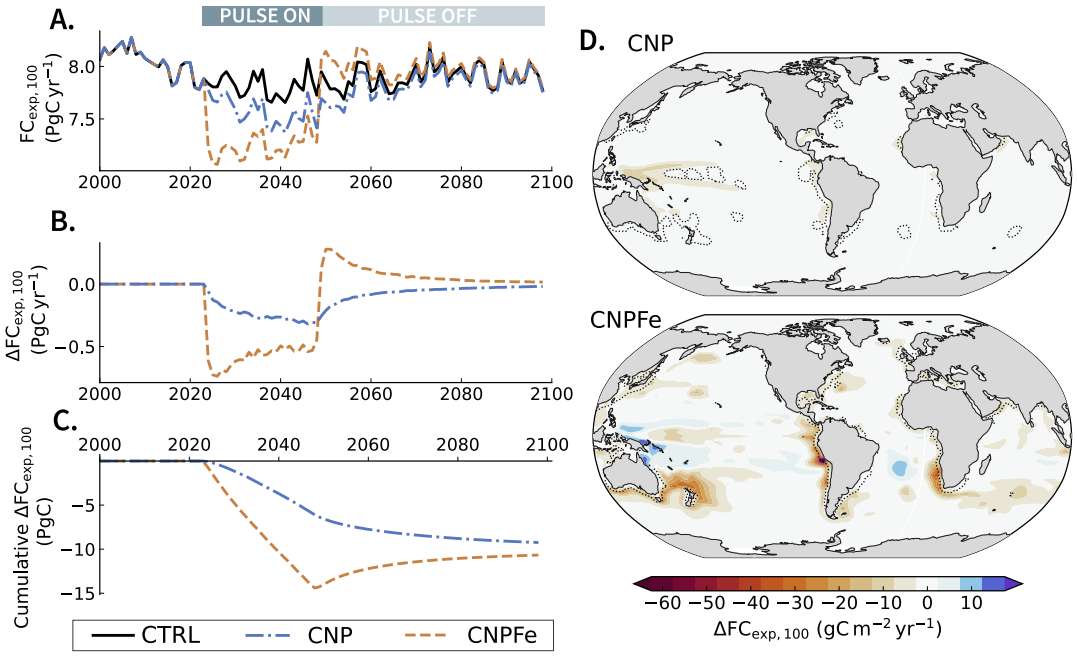

Fig. 4 Impact of seaweed nutrient limitation on carbon export flux at 100 m. Time series of (**A**) global carbon export flux at 100 m ($FC_{exp,\ 100}$) in the control simulation (RCP2.6 scenario) and in seaweed cultivation simulations under two nutrient limitation scenarios: nitrate and phosphate (CNP), and nitrate, phosphate, and iron (CNPFe). Time series of (**B**) change in global $FC_{exp,\ 100}$ (PgC yr^{-1}) and (**C**) cumulative global $FC_{exp,\ 100}$ (PgC) for the two nutrient limitation scenarios (**D**) Spatial change in $FC_{exp,\ 100}$ averaged over 25 years of cultivation relative to the control simulation (gC m^{-2} yr^{-1}). Dashed lines represent the threshold of 0.15 kgC m^{-2} yr^{-1} for seaweed production.

2.4 Seaweed iron consumption amplifies phytoplankton production decline

In the control simulation (without seaweed cultivation) under the RCP2.6 scenario, phytoplankton primary production (NPP_{PHY}) shows a climate change signal, with a global decline peaking in 2040 followed by a gradual recovery. In the idealized simulation C, where seaweed only consumes DIC (no nutrient limitation), phytoplankton production remains unaffected, showing no deviation from the control simulation. However, when N and P limitations are introduced, phytoplankton primary production decreases by up to 2 PgC yr^{-1}, decreasing by 4.8% global NPP_{PHY} compared to the control (Fig. 5, CNP). The introduction of iron limitation further exacerbates this reduction, decreasing phytoplankton primary production by up to 3.5 PgC yr^{-1} in the second year of cultivation,

corresponding to an 8% decrease in global NPP_{PHY} (Fig. 5, CNPFe). However, after cessation of cultivation, phytoplankton production recovers quickly increasing to 1.9 PgC yr^{-1} two years after cessation.

Regionally, N and P limitations trigger NPP_{PHY} declines in the western equatorial Pacific, with phytoplankton production declining by 106 gC m^{-2} yr^{-1} — equivalent to a 57% reduction (Fig.5 C and D). The addition of iron limitation intensifies this decline to 268.3 gC m^{-2} yr^{-1}, or an 81% reduction, particularly in the Southern Ocean and eastern boundary regions. However, some regions in the subtropics exhibit increased phytoplankton production of up to 90 gC m^{-2} yr^{-1}, corresponding to a 97% increase under seaweed N, P, and Fe consumption.

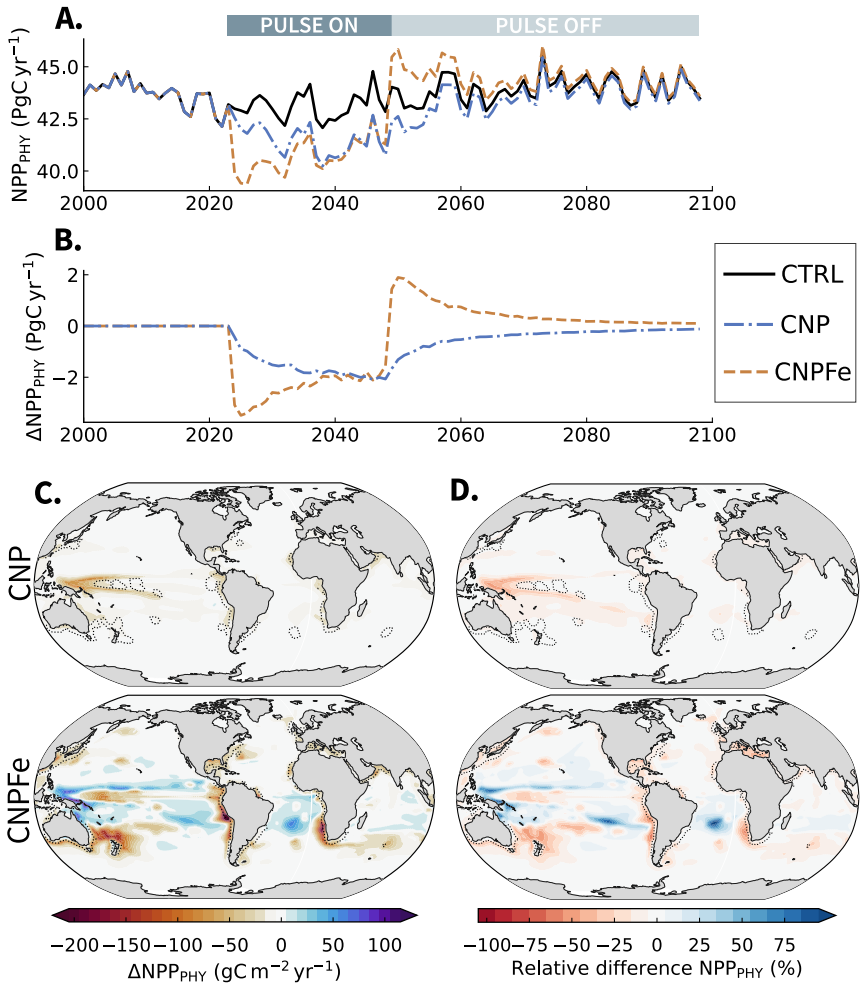

Fig. 5 Impact of seaweed nutrient limitation on phytoplankton production. Time series of (**A**) global phytoplankton net primary production (NPP_{PHY}) in the control simulation (RCP2.6 scenario) and in seaweed cultivation simulations under two nutrient limitation scenarios: nitrate and phosphate (CNP), and nitrate, phosphate, and iron (CNPFe); (**B**) change in global NPP_{PHY} in these two scenarios. Change in phytoplankton net primary production compared to control simulation (no seaweed cultivation) averaged over 25 years of cultivation in (**C**) absolute, (**D**) relative difference. Dashed lines represent the threshold of 0.15 kgC m^{-2} yr^{-1} for seaweed production.

2.5 Favorable regions for seaweed CDR effectively non-existent

Favorable regions for seaweed-based CDR were identified as regions with high afforestation potential, high CDR efficiency, and minimal environmental impacts on phytoplankton. Under nitrate and phosphate limitations, a vast area of 24 million km^2 or 20% of global EEZs, was determined to have high afforestation potential (Fig. 6 A, green). Some regions of high afforestation potential coincided with areas of high CDR flux, including the Pacific and Atlantic upwelling zones and the Southern Ocean (Fig. 6 A, magenta). Phytoplankton impacts were mostly localized in the western equatorial Pacific, likely due to upstream cultivation effects around Pacific islands. The Southern Ocean and upwelling regions stood out as optimal areas with high production, high CDR fluxes, and minimal impacts on phytoplankton.

When iron limitation is introduced, the area with high afforestation potential shrank drastically to 4 million km^2, representing 3% of global EEZs. No regions exhibited both high CDR flux and high production, except a small region in the Senegalese upwelling center (Fig. 6 B). High phytoplankton impact areas expanded, excluding most of the Southern Ocean and upwelling systems. Under N, P, and Fe limitations, regions with high CDR flux and minimal phytoplankton impact were concentrated in the western North Pacific and parts of the North Atlantic.

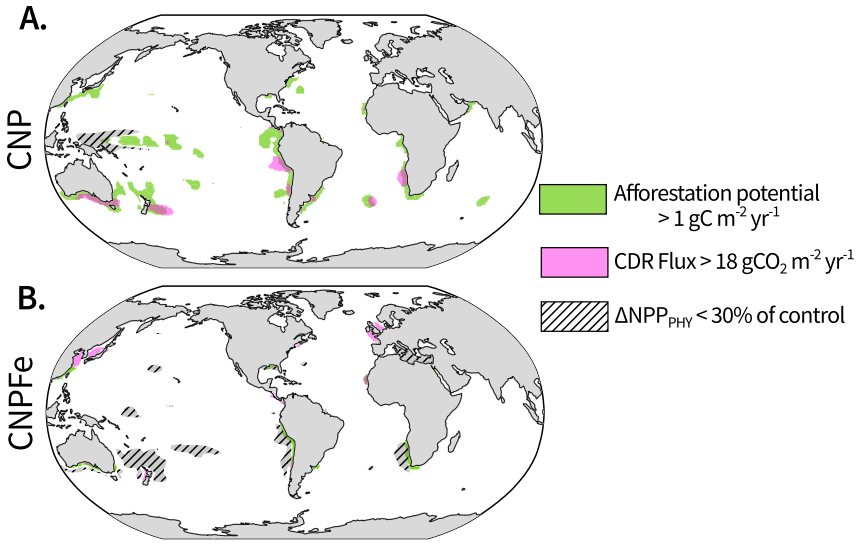

Fig. 6 Favorable seaweed cultivation regions considering nutrient limitation and phytoplankton impacts. Regions where seaweed cultivation is simulated to result in high afforestation potential (green), high CDR flux (magenta), and low phytoplankton impact (grey, hatches), under two nutrient limitation scenarios: (**A**) nitrate and phosphate, and (**B**) nitrate, phosphate, and iron.

2.6 Phosphorus demand has the greatest capacity to reduce CDR

The CDR potential of seaweed afforestation depends on both the scale of afforestation and carbon removal efficiency. Variability in nutrient demand and affinity introduces uncertainty into both afforestation potential (Fig. 7 A) and CDR potential (Fig. 7 B) via the impact on the BCP (Fig. 7 C). High nutrient affinity reflects the ability to compete more efficiently for available nutrients, thereby reducing nutrient limitation. Conversely, nutrient demand plays a key role in determining whether seaweed cultivation enhances ocean carbon uptake and provides additionality. Ultimately, the relative nutrient demands of seaweed and phytoplankton determine whether seaweed can fix more carbon than phytoplankton for a given nutrient pool.

Among the nutrients simulated, phosphorus demand introduces the greatest uncertainty into both afforestation potential (Fig. 7 A) and CDR flux (Fig. 7 B), followed by iron and then nitrogen. The lower P demand bound (C:P of 461) of seaweed can increase afforestation potential by up to 53%, a trend consistent over 25 years of cultivation. However, high P demand (C:P of 15) results in a net reduction in ocean carbon uptake, with a cumulative loss of 15 PgC over 25 years of cultivation, (i.e. negative CDR). This negative CDR flux persists, even after 50 years of cessation, due to a long-lasting BCP feedback that reduces carbon export by 58 PgC after 25 years and does not recover.

Iron demand introduces the second largest source of uncertainty. The high Fe demand bound (C:Fe ratio of 172) reduces afforestation potential by 28%, while also leading to negative CDR, with a 9.4 PgC reduction in ocean carbon uptake over 25 years, associated with a 43.6 PgC decrease in carbon export (Fig. 7 C). Conversely, low Fe demand (C:Fe ratio of 23,214) enhances both the CDR flux and efficiency, with an additional 9.8 PgC of ocean carbon uptake after 50 years of cessation, corresponding to 78% efficiency, and reduced impact on carbon export (-6.7 PgC after 25 years).

In comparison, variability in nitrogen demand has a much smaller effect on ocean afforestation potential, with projection anomalies of less than 2%. The impact of N demand on CDR flux is more pronounced. High N demand (C:N ratio of 4) results in a globally negative CDR flux, with losses of up to 3 PgC from reduced ocean carbon uptake, and a 12% reduction in global phytoplankton production. In contrast, low N demand (C:N ratio of 144) enhances CDR, with CDR efficiency reaching 70% after 50 years of cessation.

Variability in nutrient affinity also contributes to uncertainty in afforestation potential. Variations in iron affinity have the strongest effect, with high Fe affinity (K_{Fe} of 0.29 nmolFe/L) increasing afforestation potential by 85%, while low Fe affinity (K_{Fe} of 5.15 nmolFe/L) decreases it by 43% (Fig. 7, right panels). Variations in nitrogen affinity are the second most influential,

with a high affinity (K_N of 1.1) increasing afforestation by 13%, and a low affinity reducing it by 40%. Variability in phosphorus affinity has a relatively minor impact (<8%). While nutrient affinity variations do not substantially alter total global seaweed production, they do affect its regional distribution, leading to slight changes in CDR efficiency.

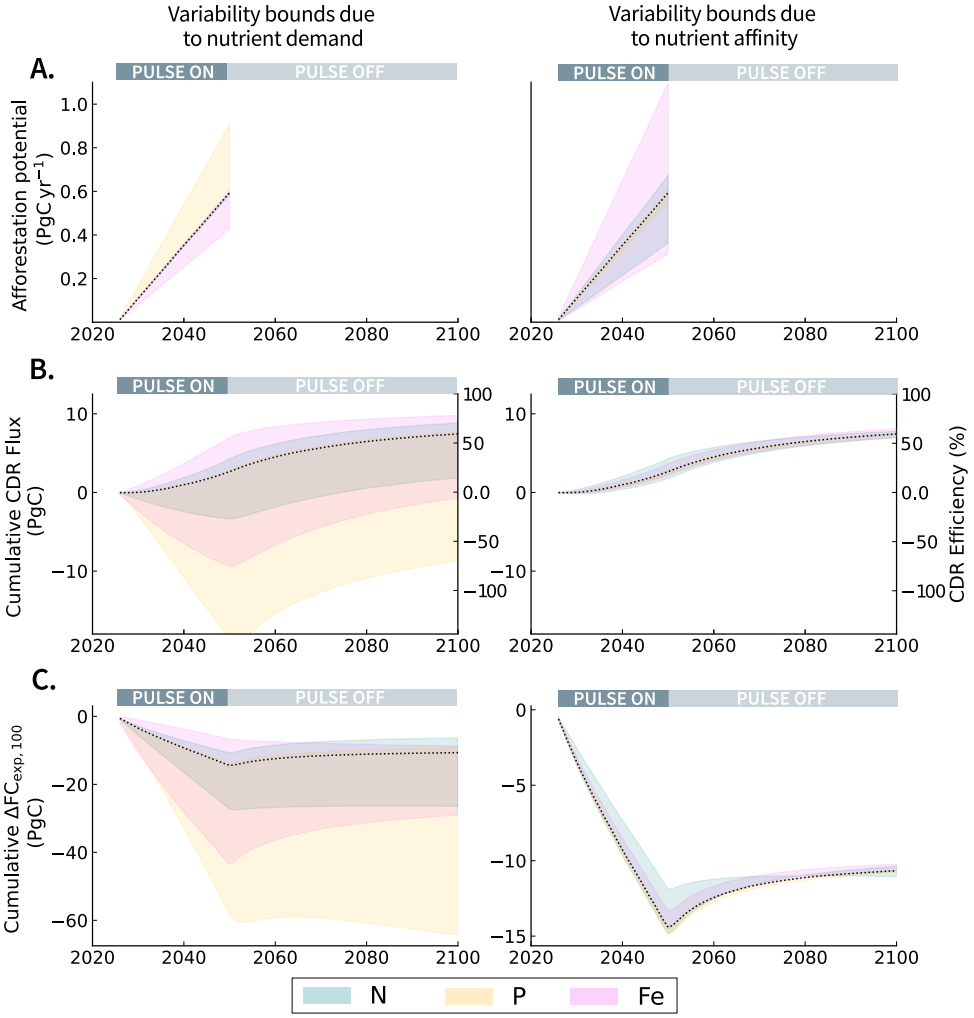

Fig. 7 Impact of nutrient demand and affinity variability on CDR potential. Bounds of N (blue), P (yellow), and Fe (pink) demands (left panels) and affinities (right panels) are shown. These influence (**A**) afforestation potential, (**B**) carbon dioxide removal (CDR) flux and CDR efficiency, and (**C**) cumulative carbon export at 100 m. Dotted lines represent the mean demand and affinity values for N, P, and Fe.

3 Discussion

3.1 Iron diminishes seaweed CDR and exacerbates environmental impacts

Iron availability is demonstrated to be a critical determinant of seaweed CDR potential, affecting both ocean afforestation potential and CDR efficiency, confirming the need to include it in

CDR discussions, as suggested by Paine et al. (2023) [6]. Iron is a key micronutrient required for photosynthesis and cellular metabolism in both phytoplankton and seaweed [6]. When seaweed iron requirements and uptake kinetics are accounted for in our simulations, both projected ocean afforestation potential and CDR efficiency decline (Fig. 2 and 3).

Under macronutrient limitation, simulated CDR efficiency is 82% after 25 years of cultivation, aligning with previous global modeling studies on multi-centennial timescales [11] but exceeding decadal estimates, which likely underestimate efficiency due to incomplete air-sea equilibration [10]. This also falls within the 7–50% reduction in CDR efficiency due to nutrient reallocation estimated from natural analogs [14]. Under iron-limited conditions, CDR efficiency is further diminished, with 20% of the ocean becoming counterproductive and exhibiting reduced ocean carbon uptake instead of enhancement (Fig. 3). Notably, regions that previously exhibited the highest CDR flux under only nitrogen and phosphorus limitations—such as the Southern Ocean and upwelling zones—experience reduced or even negative CDR flux when iron limitation is included (up to -50 gCO_2 m^{-2} yr^{-1}) (Fig. 3). This global reduction in CDR flux, along with the emergence of regions with negative CDR, is largely driven by stronger BCP feedback under iron limitation (Fig. 4). Since iron is already a limiting nutrient in many ocean regions, the additional iron demand from seaweed cultivation further depletes iron availability for phytoplankton, thereby constraining productivity. Iron limitation also alters the temporal dynamics of seaweed cultivation. Under iron limitation, CDR flux and phytoplankton primary production anomalies peak within just two years of cultivation, followed by a rebound effect after cultivation ceases (Fig. 5 and 4). This rebound is attributed to the short seawater residence time of iron, with a similar response simulated in ocean fertilization experiments [15].

Iron limitation not only reduces CDR potential but also intensifies the impact of seaweed cultivation on phytoplankton (Fig. 5). Phytoplankton responses are highly variable, with production declines in some regions and increases in others due to a shift in nutrient co-limitations. These changes are likely to cascade through marine ecosystems, disrupting trophic structures and affecting zooplankton, fish, and other organisms reliant on phytoplankton, the foundation of the marine food web [16].

Our simulations highlight the complexity of identifying optimal regions for ocean afforestation. While seaweed cultivation is often assumed to have high CDR potential due to the vast habitable areas within EEZs [17], accounting for biogeochemical feedbacks, nutrient limitations, and phytoplankton impacts, is required to identify favorable deployment regions. Simulated high afforestation potential under macronutrient limitation (Fig. 6) aligns with production hotspots

identified by Arzeno-Soltero et al. [12]. However, exceptions were noted in the North Pacific and Atlantic, where our model simulations showed lower production, likely due to surface nutrient biases in the NEMO-PISCES model (see Fig. S1 in Supplementary Materials). The Southern Ocean and upwelling zones emerged as favorable regions when only nitrate and phosphate limitations were considered, offering high production and CDR flux with minimal environmental impacts. These areas overlap with regions identified by He et al. [18] as optimal for ocean alkalinity enhancement (OAE), suggesting synergies between ocean-based CDR strategies in regions where air-sea CO_2 transfer timescale exceeds surface residence time [19]. Iron limitation, however, drastically diminishes favorable regions and excludes key regions such as the Southern Ocean and upwelling systems. This underscores the challenge of optimizing production while maintaining high CDR efficiency and minimizing environmental impacts, with iron emerging as a key limitation in this paradigm.

3.2 Sensitivity to nutrient demand and affinity

Nutrient affinity plays a critical role in modulating the afforestation potential by determining seaweed-phytoplankton nutrient competition dynamics. Previous studies found that nutrient affinity variability had limited influence on afforestation potential compared to other biophysical constraints but did not explicitly account for competition with phytoplankton [12]. Incorporating this competition, we demonstrate that nutrient affinity, particularly iron affinity, substantially affects afforestation potential.

Our projections also highlight the role of nutrient demand in determining the efficacy of seaweed cultivation-based CDR (Fig. 7). For seaweed to fix more carbon than phytoplankton using the same available nutrient pool, it must be more nutrient efficient. Any carbon fixation advantage depends on how much lower seaweed nutrient demand is compared to phytoplankton [9], as well as on the proportion of nutrients that remain unused by the BCP. Together, these factors determine overall CDR efficiency. Lower nutrient demands result in fewer nutrients being diverted from the BCP, and a smaller BCP feedback (Fig. 7 B and C). Variability in phosphorus demand has the most substantial effect on CDR efficiency, causing uncertainties ranging from -70% to 61% in global efficiency, followed by iron and nitrogen. In comparison, Wu et al. [11] found that a 20% increase or decrease in nitrogen demand leads to a 10% change in global CDR efficiency during continuous cultivation on a centennial scale. In contrast, our analysis using published stoichiometric ratios revealed a much larger range, with an increase of 800% and a reduction of 77% in N demand, resulting in a decrease of 45% and an increase of 10% in CDR efficiency, respectively.

This reveals a fundamental trade-off: maximizing CDR efficiency requires low nutrient demand and high nutrient affinity, yet low seaweed nutrient demand is typically found in nutrient-poor environments [9], which inherently limits seaweed production potential. Optimizing seaweed cultivation for climate mitigation requires a careful balance between maximizing CDR efficiency and generating substantial seaweed biomass. Future efforts should carefully consider these trade-offs when developing effective and sustainable seaweed-based strategies.

Our findings underscore the need for iron demand and affinity to be included in projections of seaweed-based CDR. Failing to account for such nutrient dynamics is likely to result in erroneous estimates of the potential of seaweed-based CDR as a mitigation strategy.

4 Materials and Methods

4.1 Model

Simulations were performed using version 3.6 of the Nucleus for European Modelling of the Ocean (NEMO), which integrates the Louvain-La-Neuve Sea Ice Model (LIM) version 3 [20] and the Pelagic Interaction Scheme for Carbon and Ecosystem Studies (PISCES) biogeochemical model version 2 [21]. The PISCES model incorporates various forms of carbon, including dissolved inorganic carbon, dissolved organic carbon, particulate inorganic carbon (calcite), and particulate organic carbon, as well as living compartments such as nanophytoplankton, diatoms, microzooplankton, and mesozooplankton. It also includes total alkalinity and essential marine nutrients such as nitrate, ammonium, phosphate, silicate, and iron. The PISCES model represents four sources of dissolved iron: dust deposition, riverine input, hydrothermal vents, and sediment resuspension. Scavenging is computed following Parekh et al. [22], with scavenging rates dependent on particle concentrations. The model includes a representation of colloidal losses of dissolved Fe via the aggregation of dissolved organic material, as described by Aumont et al. [21]. It assumes a constant ligand concentration and employs a quota approach for Fe stoichiometry in organic matter, with the regeneration efficiency of particulate Fe dependent on stoichiometry. PISCES includes two sizes of particulate iron pools [23]. Air-sea CO_2 fluxes follow the protocols of the Ocean Model Intercomparison Project [24], with gas exchange determined by the air-sea partial pressure gradient and an instantaneous gas transfer velocity parameterized based on 10 m atmospheric wind speed [25, 26].

NEMO-PISCES simulations were performed using a 2° global ocean configuration (ORCA2). This resolution permitted centennial scale simulations that extensively explore seaweed nutrient demand and affinity parameter space.

4.2 Simulations

Seaweed production

Seaweed production in NEMO-PISCES is simulated as the uptake of DIC and nutrients in EEZs. EEZ definitions are based on the Maritime Boundaries Geodatabase, version 11 (Flanders Marine Institute, 2019, available at https://www.marineregions.org). Production is continuous and is considered immediately harvested and permanently sequestered with no associated carbon emissions. Consequently, there is no remineralization of seaweed biomass. Seaweed production is temperature, light, and nutrient-limited, but explicit seaweed biomass is not represented (see Supplementary Materials for detailed production functions). Two types of nutrient limitations and consumption were tested, alongside simulations that assume no nutrient demand:

- **DIC only (C):** Seaweed carbon, no nutrient limitation and consumption.
- **Macronutrient only (CNP):** Seaweed carbon, nitrate, and phosphate consumption and limitation.
- **Macronutrient and iron (CNPFe):** Seaweed carbon, nitrate, phosphate, and iron consumption and limitation.

Moreover, we conducted two sets of seaweed cultivation simulations:

- **Afforestation potential simulations:** In these simulations, we use a free production approach, with homogeneous farm density (Fig. 8 A). A unique scaling factor, representing a maximum production rate of 0.09 mmolC m^{-3} d^{-1}, is applied consistently across all simulations. This scaling enables the reference scenario, which assumes no nutrient limitation (simulation C), to achieve a global seaweed production of 0.5 $\mathrm{PgC\,yr^{-1}}$. This approach allows us to test the relative effects of macronutrient (N,P), and Fe limitation on afforestation potential.
- **CDR efficiency and phytoplankton impact simulations:** In these simulations, we use a globally constrained production approach, indicative of higher farm density in nutrient-rich regions that support higher production (Fig. 8 B). Each scenario has a specific scaling of the maximal per-area production of seaweed to constrain global production to 0.5 $\mathrm{PgC\,yr^{-1}}$ (see Table 1). This method was used to compare CDR efficiency under conditions of similar global seaweed production.

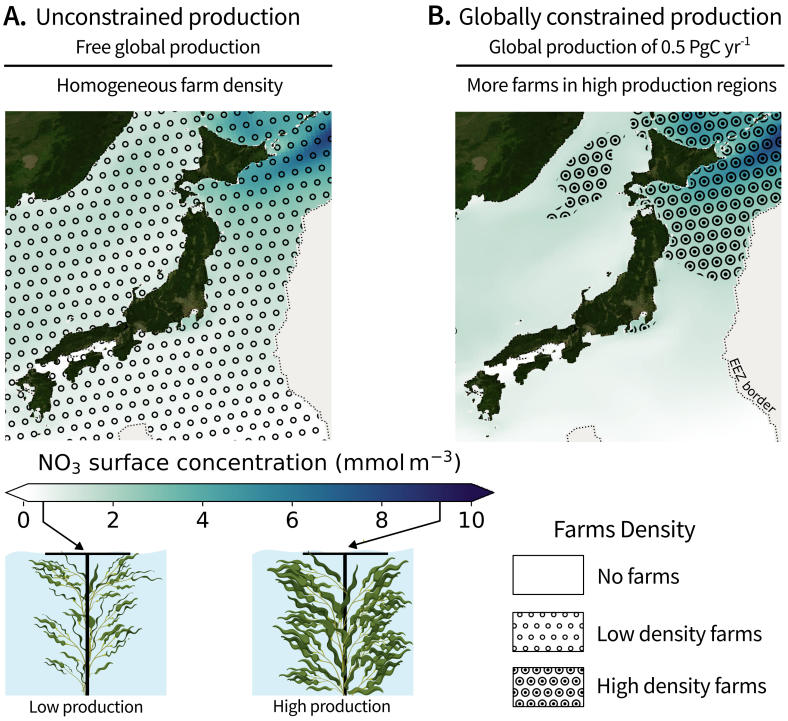

Fig. 8 Schematic of the two simulation sets. The left panel (**A**) illustrates unconstrained production, where a uniform farm density across global EEZs is used to estimate the afforestation potential. The right panel (**B**) depicts globally constrained production, where farm density is concentrated in nutrient-rich regions to achieve global production of 0.5 PgC yr^{-1}. These simulations are used to assess CDR efficiency and impacts on phytoplankton productivity at a fixed global production level.

Table 1 Descriptions of the maximal per-area seaweed production in C, CNP and CNPFe simulations, scaled to constrain global seaweed production to 0.5 PgC yr^{-1}.

Name	Maximal production (mmolC m^{-3} d^{-1})
C	0.09
CNP	0.67
CNPFe	3.72

Nutrient demands and affinities

The nutrient demands are inversely proportional to the carbon-to-nutrient ratios (C:N, C:P, and C:Fe) of seaweed biomass. To explore the variability in seaweed nutrient demand, we compiled published seaweed C:N:P stoichiometric ratios (Fig. 2) [9, 27–31] and C:Fe [32–34], selecting temperate brown seaweed species including *laminaria digitata, macrocystis pyrifera, laminaria japonica, laminaria hyperborea*, and *laminaria saccharina*. To account for potential variability not captured in the dataset, we set the maximum and minimum values 25% higher and lower, respectively, than the published extremes (Table 2).

The bounds we employed for half-saturation constants are based on published uptake rates for nitrate [35–37], phosphate [38, 39], and iron [6, 40] (Table 2). As with stoichiometric ratios, maximum (resp. minimum) values were chosen to be 25% larger (resp. smaller). Values of K_{NO_3} are consistent with those used in previous studies [12].

These simulations, which incorporate mean, minimal, and maximal values of stoichiometric ratios (demand) and half-saturation constants (affinity) reported in the literature, provide insights into how variations in these biological parameters influence the production potential, the CDR efficiency and the impact on phytoplankton. While it may be unrealistic for global seaweed cultivation to consistently adopt the extreme C:N:P:Fe ratios and half-saturation constants, exploring such scenarios permits the assessment of the sensitivity of afforestation potential and CDR efficiency to these parameters at both global and regional scales.

Table 2 Descriptions of the biological parameters used in this study, mean, minimal (min.), and maximal (max.) values. Note that nutrient affinity is inversely proportional to the half-saturation constant (K_s), and the nutrient demand is the inverse of the carbon-to-nutrient ratio.

	Parameter	Units	Mean value	Min. value	Max. value	Ref
Half-saturation constant	K_{NO_3}	µmolN/L	2	1.1	18.1	[11]
	K_{PO_4}	µmolP/L	0.1	0.06	6.5	[39, 41]
	K_{Fe}	nmolFe/L	1.56	0.29	5.15	[6]
Carbon-to-nutrient ratio	q_{Fe}	molC/molFe	3346	172	23214	[32–34]
	q_{NO_3}	molC/molN	17	4	144	[9, 27–31]
	q_{PO_4}	molC/molP	269	15	461	

4.3 Evaluation of simulated nutrient fields

PISCES exhibits no systematic bias in upper ocean nitrate, phosphate, and iron concentrations, performing well in reproducing large-scale nutrient distributions [21]. Among the FeMIP models, PISCES demonstrates one of the highest correlation values for dissolved iron concentrations (PISCES1 in Tagliabue et al., 2016 [23]), indicating reasonable agreement with observational datasets. However, discrepancies remain in certain regions. The largest biases for nitrate and phosphate are found in the North Pacific, with root mean square errors (RMSE) of up to 8.5 mmol m^{-3} for nitrate and 0.8 mmol m^{-3} for phosphate (Fig. S1 in Supplementary Materials). For dissolved iron, the most significant deviations occur in the Arctic and North Atlantic, with RMSE of up to 5 μmol m^{-3} (Fig. S1 in Supplementary Materials).

4.4 Scenarios

Seaweed cultivation was performed for 25 years (2025-2050), followed by a subsequent 50-year period without any cultivation (2050-2100). We ran offline biogeochemical model simulations with ocean physics derived from the ESM IPSL-CM5A-LR. The atmospheric CO_2 concentration is prescribed with the Representative Concentration Pathway (RCP) 2.6 scenario, a low-emission scenario. Under this scenario, atmospheric CO_2 concentration peaks at 443 ppm in 2052 and decreases to 421 ppm by 2100.

Acknowledgments

The authors thank Olivier Torres for his help with the model and the IPSL modeling group for the software infrastructure, which facilitated model simulations and analysis. The authors would like to thank Judith Hauck, Paul Halloran, and Laure Resplandy for their feedback on an earlier version of the manuscript and insightful discussions.

Funding. Authors received funding from the ENS-Chanel research chair. Simulations were carried out with computational resources from TGCC through a GENCI/DARI grant (gen0040). Model output was analyzed on the IPSL Prodiguer-Ciclad cluster, a facility supported by CNRS, Sorbonne Université, and Labex L-IPSL, the latter being funded by ANR (Grant ANR-10-LABX-0018) and European FP7 IS-ENES2 project (Grant 312979).

Author contributions. All authors contributed to conceiving this study. M.B. performed the literature review, the simulations, the model output analysis, and produced the figures. All authors contributed ideas and participated in discussions of the results. L.B, L.K., and D.T.H. provided supervision. M.B. wrote the initial draft, and all authors contributed to the writing and editing.

Competing interests. The authors declare that they have no competing interests.

Data availability. All data needed to evaluate the conclusions in the paper are present in the paper and/or the Supplementary Materials. The data that support the findings of this study are openly available at the following URL/DOI ().

References

[1] Smith, S.M., Geden, O., Gidden, M.J., Lamb, W.F., Nemet, G.F., Minx, J.C., Buck, H., Burke, J., Cox, E., Edwards, M.R., Fuss, S., Johnstone, I., Müller-Hansen, F., Pongratz, J., Probst, B.S., Roe, S., Schenuit, F., Schulte, I., Vaughan, N.: E. In: Smith, S.M., Geden, O., Gidden, M.J., Lamb, W.F., Nemet, G.F., Minx, J.C., Buck, H., Burke, J., Cox, E., Edwards, M.R., Fuss, S., Johnstone, I., Müller-Hansen, F., Pongratz, J., Probst, B.S., Roe, S., Schenuit, F., Schulte, I., Vaughan, N. (eds.) The State of Carbon Dioxide Removal 2024 - 2nd Edition., Doi 10.17605/osf.io/f85qj edn.

[2] Mann, K.H.: Seaweeds: Their productivity and strategy for growth. Science **182**(4116), 975–81 https://doi.org/10.1126/science.182.4116.975.

[3] Cai, J.: Seaweeds and microalgae: An overview for unlocking their potential in global aquaculture development. FAO Fisheries and Aquaculture Circular **1229** https://doi.org/10.4060/cb5670en.

[4] Boyd, P.W., Bach, L.T., Hurd, C.L., Paine, E., Raven, J.A., Tamsitt, V.: Potential negative effects of ocean afforestation on offshore ecosystems. Nature Ecology & Evolution **April**, 1–9 https://doi.org/10.1038/s41559-022-01722-1.

[5] Gallagher, J.B., Shelamoff, V., Layton, C.: Seaweed ecosystems may not mitigate co2 emissions. ICES Journal of Marine Science, February, 011 https://doi.org/10.1093/icesjms/fsac011.

[6] Paine, E.R., Boyd, P.W., Strzepek, R.F., Ellwood, M., Brewer, E.A., Diaz-Pulido, G., Schmid, M., Hurd, C.L.: Iron limitation of kelp growth may prevent ocean afforestation. Communications Biology **6**(1), 1–9 https://doi.org/10.1038/s42003-023-04962-4.

[7] Chen, B., Zou, D., Yang, Y.: Increased iron availability resulting from increased co2 enhances carbon and nitrogen metabolism in the economical marine red macroalga pyropia haitanensis (rhodophyta). Chemosphere **173**, 444–451 (2017)

[8] Browning, T.J., Moore, C.M.: Global analysis of ocean phytoplankton nutrient limitation reveals high prevalence of co-limitation. Nature Communications **14**(1), 5014 (2023)

[9] Sheppard, E.J., Hurd, C.L., Britton, D.D., Reed, D.C., Bach, L.T.: Seaweed biogeochemistry: Global assessment of c:n and c:p ratios and implications for ocean afforestation.

Journal of Phycology **59**(5), 879–92 https://doi.org/10.1111/jpy.13381.

[10] Berger, M., Kwiatkowski, L., Ho, D.T., Bopp, L.: Ocean dynamics and biological feedbacks limit the potential of macroalgae carbon dioxide removal. Environmental Research Letters https://doi.org/10.1088/1748-9326/acb06e.

[11] Wu, J., Keller, D.P., Oschlies, A.: Carbon dioxide removal via macroalgae open-ocean mariculture and sinking: an earth system modeling study **14**(1), 185–221 https://doi.org/10.5194/esd-14-185-2023 . Publisher: Copernicus GmbH. Accessed 2023-07-26

[12] Arzeno, I.S., Saenz, B., Frieder, C., Long, M., DeAngelo, J., Davis, S., Davis, K.: Large global variations in the carbon dioxide removal potential of seaweed farming due to biophysical constraints. Communications Earth & Environment **4** https://doi.org/10.1038/s43247-023-00833-2.

[13] Ocean Visions and Monterey Bay Aquarium Research Institute: Answering Critical Questions About Sinking Macroalgae for Carbon Dioxide Removal: A Research Framework to Investigate Sequestration Efficacy and Environmental Impacts (2022)

[14] Bach, L.T., Tamsitt, V., Gower, J., Hurd, C.L., Raven, J.A., Boyd, P.W.: Testing the climate intervention potential of ocean afforestation using the great atlantic sargassum belt. Nature Communications **12**(1), 2556 (2021)

[15] Aumont, O., Bopp, L.: Globalizing results from ocean in situ iron fertilization studies. Global Biogeochemical Cycles **20**(2) (2006)

[16] Tagliabue, A., Twining, B.S., Barrier, N., Maury, O., Berger, M., Bopp, L.: Ocean iron fertilization may amplify climate change pressures on marine animal biomass for limited climate benefit. Global Change Biology **29**(18), 5250–5260 (2023) https://doi.org/10.1111/gcb.16854 . _eprint: https://onlinelibrary.wiley.com/doi/pdf/10.1111/gcb.16854

[17] Froehlich, H.E., Afflerbach, J.C., Frazier, M., Halpern, B.S.: Blue growth potential to mitigate climate change through seaweed offsetting **29**(18), 3087–30933 https://doi.org/10.1016/j.cub.2019.07.041

[18] He, J., Tyka, M.D.: Limits and CO_2 equilibration of near-coast alkalinity enhancement. Biogeosciences **20**(1), 27–43 (2023) https://doi.org/10.5194/bg-20-27-2023 . Publisher: Copernicus GmbH

[19] Kwiatkowski, L., Berger, M., Bopp, L., Doléac, S., Ho, D.T.: Contrasting carbon dioxide removal potential and nutrient feedbacks of simulated ocean alkalinity enhancement and macroalgae afforestation. Environmental Research Letters **18**(12), 124036 https://doi.org/10.1088/1748-9326/ad08f9.

[20] Fichefet, T., Maqueda, M.A.M.: Sensitivity of a global sea ice model to the treatment of ice thermodynamics and dynamics. Journal of Geophysical Research: Oceans **102**(C6), 12609–46 https://doi.org/10.1029/97JC00480.

[21] Aumont, O., Ethé, C., Tagliabue, A., Bopp, L., Gehlen, M.: PISCES-v2: an ocean biogeochemical model for carbon and ecosystem studies **8**(8), 2465–2513 https://doi.org/10.5194/gmd-8-2465-2015 . Number: 8

[22] Parekh, P., Follows, M.J., Boyle, E.: Modeling the global ocean iron cycle. Global biogeochemical cycles **18**(1) (2004)

[23] Tagliabue, A., Aumont, O., DeAth, R., Dunne, J.P., Dutkiewicz, S., Galbraith, E., Misumi, K., Moore, J.K., Ridgwell, A., Sherman, E., *et al.*: How well do global ocean biogeochemistry models simulate dissolved iron distributions? Global Biogeochemical Cycles **30**(2), 149–174 (2016)

[24] Orr, J.C., Najjar, R.G., Aumont, O., Bopp, L., Bullister, J.L., Danabasoglu, G., Doney, S.C.: Biogeochemical protocols and diagnostics for the cmip6 ocean model intercomparison project (omip. Geoscientific Model Development **10**(6), 2169–99 https://doi.org/10.5194/gmd-10-2169-2017.

[25] Wanninkhof, R.: Relationship between wind speed and gas exchange over the ocean **97**, 7373–7382 https://doi.org/10.1029/92JC00188 . Number: C5

[26] Ho, D.T., Law, C.S., Smith, M.J., Schlosser, P., Harvey, M., Hill, P.: Measurements of air-sea gas exchange at high wind speeds in the southern ocean: Implications for global parameterizations **33**(16) https://doi.org/10.1029/2006GL026817 . _eprint: https://onlinelibrary.wiley.com/doi/pdf/10.1029/2006GL026817. Accessed 2024-02-27

[27] Tussenbroek, B.I.v.: Seasonal growth and composition of fronds of macrocystis pyrifera in the falkland islands. Marine Biology **100**(3), 419–30 https://doi.org/10.1007/BF00391158.

[28] Zimmerman, R., Kremer, J.: In situ growth and chemical composition of the giant kelp, macrocystis pyrifera: Response to temporal changes in ambient nutrient availability. Marine Ecology Progress Series **27**, 277–85 https://doi.org/10.3354/meps027277.

[29] Johnson, K.S., Gordon, R.M., Coale, K.H.: What controls dissolved iron concentrations in the world ocean? Marine Chemistry **57**(3), 137–61 https://doi.org/10.1016/S0304-4203(97)00043-1.

[30] Gevaert, F., Janquin, M.-A., Davoult, D.: Biometrics in laminaria digitata: A useful tool to assess biomass, carbon and nitrogen contents. Journal of Sea Research **60**(3), 215–19 https://doi.org/10.1016/j.seares.2008.06.006.

[31] Stewart, H., Fram, J., Reed, D., Williams, S., Ma Brzezinski, S.M., Gaylord, B.: Differences in Growth, Morphology and Tissue Carbon and Nitrogen of Macrocystis Pyrifera within and at the Outer Edge of a Giant Kelp Forest in, California, USA. Marine Ecology Progress Series 375 (January):101–12. https://doi.org/10.3354/meps07752.

[32] North, W.J.: Trace metals in giant kelp, macrocystis. American Journal of Botany **67**(7), 1097–1101 (1980)

[33] Schiener, P., Black, K.D., Stanley, M.S., Green, D.H.: The seasonal variation in the chemical composition of the kelp species laminaria digitata, laminaria hyperborea, saccharina latissima and alaria esculenta. Journal of applied phycology **27**, 363–373 (2015)

[34] Sharma, S., Neves, L., Funderud, J., Mydland, L.T., Øverland, M., Horn, S.J.: Seasonal and depth variations in the chemical composition of cultivated saccharina latissima. Algal Research **32** https://doi.org/10.1016/j.algal.2018.03.012.

[35] Chapman, A.R.O., Markham, J.W., Lüning, K.: Effects of nitrate concentration on the growth and physiology of laminaria saccharina (phaeophyta) in culture1,2 **14**(2), 195–198 https://doi.org/10.1111/j.1529-8817.1978.tb02448.x . _eprint: https://onlinelibrary.wiley.com/doi/pdf/10.1111/j.1529-8817.1978.tb02448.x. Accessed 2023-07-10

[36] Haines, K.C., Wheeler, P.A.: Ammoniun and nitrate uptake by the marine macrophytes hypnea musvuformis (rhodophyta) and macrocystis pyrifera (phaeophyta)1, 2 **14**(3), 319–324 https://doi.org/10.1111/j.1529-8817.1978.tb00305.x . _eprint:

https://onlinelibrary.wiley.com/doi/pdf/10.1111/j.1529-8817.1978.tb00305.x. Accessed 2024-05-24

[37] Zhang, J., Wu, W., Ren, J., Lin, F.: A model for the growth of mariculture kelp saccharina japonica in sanggou bay, china **8**, 273–283 https://doi.org/10.3354/aei00171 . Accessed 2023-12-04

[38] Pedersen, M., Borum, J., Leck Fotel, F.: Phosphorus dynamics and limitation of fast- and slow-growing temperate seaweeds in oslofjord, norway **399**, 103–115 https://doi.org/10.3354/meps08350 . Accessed 2024-03-22

[39] Ozaki, A., Mizuta, H., Yamamoto, H.: Physiological differences between the nutrient uptakes of kjellmaniella crassifolia and laminaria japonica (phaeophyceae). Fisheries science **67**(3), 415–419 (2001)

[40] Manley, S.L.: Iron uptake and translocation by *Macrocystis pyrifera* **68**(4), 914–918 https://doi.org/10.1104/pp.68.4.914 . Accessed 2024-02-29

[41] Pedersen, M., Filbee-dexter, K., Frisk, N., Sarossy, Z., Wernberg, T.: Carbon sequestration potential increased by incomplete anaerobic decomposition of kelp detritus **660**, 53–67 https://doi.org/10.3354/meps13613

[42] Bowie, G.L., Mills, W.B., Porcella, D.B., Campbell, C.L., Pagenkopf, J.R., Rupp, G.L., Johnson, K.M., Chan, P.W., Gherini, S.A., Chamberlin, C.E., et al.: Rates, constants, and kinetics formulations in surface water quality modeling (1985)

[43] Martins, I., Marques, J.: A model for the growth of opportunistic macroalgae (enteromorpha sp.) in tidal estuaries. Estuarine, Coastal and Shelf Science **55**(2), 247–257 (2002)

[44] Breeman, A.: Relative importance of temperature and other factors in determining geographic boundaries of seaweeds: experimental and phenological evidence. Helgoländer Meeresuntersuchungen **42**, 199–241 (1988)

[45] Kirk, J.T.: Light and Photosynthesis in Aquatic Ecosystems. Cambridge university press, ??? (1994)

[46] Reagan, J.R., Boyer, T.P., García, H.E., Locarnini, R.A., Baranova, O.K., Bouchard, C.,

548 Cross, S.L., Mishonov, A.V., Paver, C.R., Seidov, D., Wang, Z., Dukhovskoy, D.: World
549 Ocean Atlas 2023. Dataset: NCEI Accession 0270533 (2023)

550 [47] GEOTRACES Intermediate Data Product Group. The GEOTRACES Intermediate Data
551 Product 2021 version 2 (IDP2021v2). doi:10.5285/ff46f034-f47c-05f9-e053-6c86abc0dc7e
552 (2023)

Supplementary Materials for

Efficacy of seaweed-based carbon dioxide removal reduced by iron limitation and nutrient competition with phytoplankton

Manon Berger *et al.*

*Corresponding author: Manon Berger, manon.berger@lmd.ipsl.fr

This PDF file includes:

Supplementary Text

Seaweed production model

The macroalgal production rate is modulated by temperature, light, and nutrient affinity. The growth rate function is defined for each nutrient limitation scenario in Table 1. The temperature limiting function ($f(T)$) used is an optimum curve following Bowie et al. [42], also used by the MOS model reported in Wu et al. [11].

$$f(T) = e^{-2.4 \cdot X_T^2}$$

Where X_T verifies,

$$X_T = \frac{T - T_{opt}}{T_X - T_{opt}},$$

$$T_x = \{T_{min},\ T_w \leq T_{opt}\ T_{max},\ T_w > T_{opt}$$

T_{opt} is set to 20°C [37,43], T_{min} to 0°C [43], and T_{max} to 35°C [44].

Light limiting function ($h(I)$) follows Kirk, 1994 [45], also used by MOS model reported in Wu et al. [11], with I_{opt} set to 180 W m^{-2} [37].

$$h(I) = \frac{I}{I_{opt}} e^{1 - \frac{I}{I_{opt}}}$$

Nutrient limitations follow the Michaelis-Menten equation for nitrate, phosphate [11-12], and iron [7] (see main text for half saturation constants).

$$L_{lim}^{N,P} = min\left(L_{NO_3}, L_{PO_4}\right), \quad L_{lim}^{N,P,Fe} = min\left(L_{NO_3}, L_{PO_4}, L_{Fe}\right)$$

$$L_{NO_3} = \frac{NO_3}{NO_3 + K_{NO_3}}, \quad L_{PO_4} = \frac{PO_3}{PO_4 + K_{PO_4}}, \quad L_{Fe} = \frac{Fe}{Fe + K_{Fe}}$$

Experiments	Seaweed production functions	Tracer consumption
C	$G = g_{scale} \cdot f(T) \cdot h(I)$	ΔDIC
CNP	$G = g_{scale} \cdot f(T) \cdot h(I) \cdot L_{lim}^{N,P}$	$\Delta DIC, \Delta NO_3^-, \Delta PO_4^{2-}, \Delta Fe$
CNPFe	$G = g_{scale} \cdot f(T) \cdot h(I) \cdot L_{lim}^{N,P,Fe}$	$\Delta DIC, \Delta NO_3^-, \Delta PO_4^{2-}, \Delta Fe$

Table S1. Production functions and elements consumed by seaweed cultivation in simulations C, CNP, and CNPFe.

Simulated surface nutrients

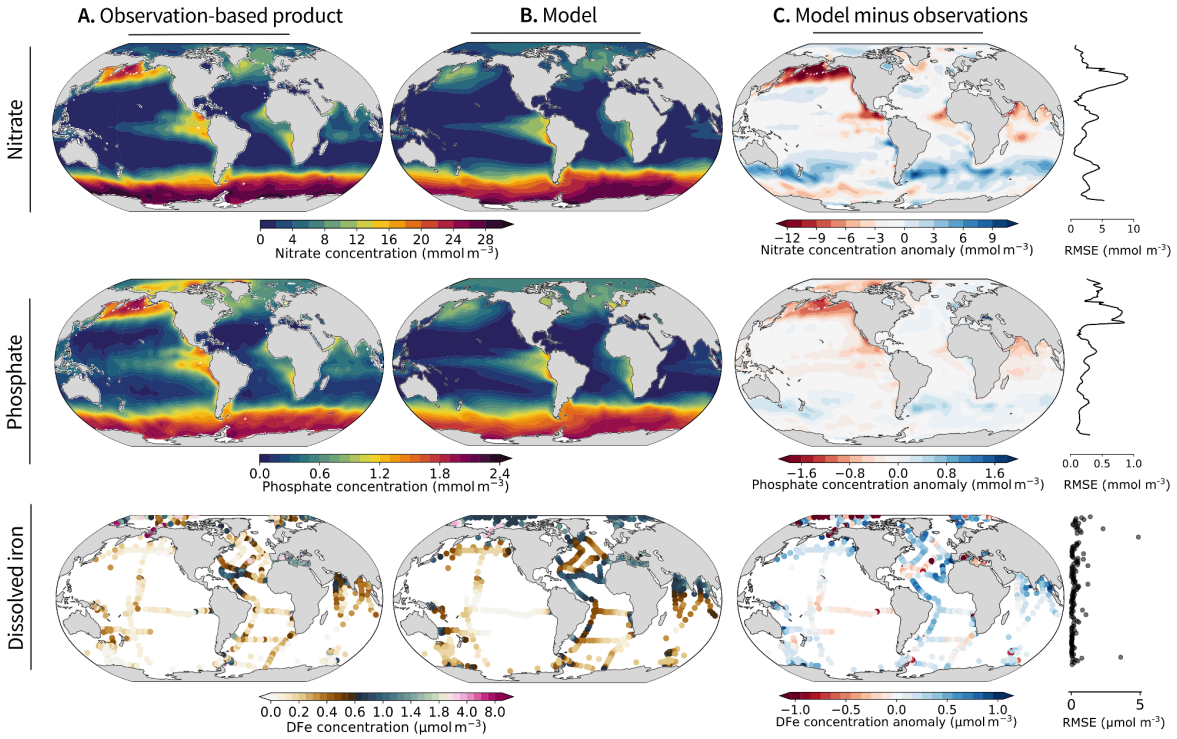

Fig. S2. (A) Observed upper 100 m nitrate and phosphate concentrations from the World Ocean Atlas [46], and iron concentrations from GEOTRACES IDP 2021 [47]. **(B)** Simulated upper 100 m nitrate, phosphate, and dissolved iron concentrations. **(C)** Differences between simulated and observation-based nutrient concentrations, and the zonal root mean square error (RMSE).